The effect of subgrid-scale models on the near wall vortices: *A priori* tests

Gwenaël Hauët,[a] Carlos B. da Silva, and José C. F. Pereira
Instituto Superior Técnico, Pav. Mecânica I, 1° Andar/esq./LASEF, Av. Rovisco Pais, 1049-001 Lisboa, Portugal

(Received 22 December 2006; accepted 26 March 2007; published online 29 May 2007)

Direct numerical simulation of a turbulent channel flow at $\mathrm{Re}_\tau=180$ is used to analyze the resolved enstrophy dissipation caused by the subgrid-scale (SGS) models. The *SGS enstrophy dissipation* attains a minimum (forward scatter) at about $y^+\approx 8$ and a backscatter region for $y^+<6$, and is correlated with the high-speed streaks. *A priori* tests show that in the buffer layer, of all the models considered, the dynamic Smagorinsky, filtered structure function, and scale-similarity models display the smallest amount of resolved enstrophy dissipation, whereas the Smagorinsky and mixed models are the most dissipative. © *2007 American Institute of Physics*. [DOI: 10.1063/1.2732455]

One of the most impressive achievements of large-eddy simulations (LES) consists of the possibility of obtaining unsteady information from turbulent flows, usually associated with the larger, most energetic scales of motion. This information is directly connected with the presence of long lived, coherent regions of concentrated enstrophy: the coherent vortices.

It is known for some time that different subgrid-scale (SGS) models lead to differences in the topology, phase and life time of the vortices obtained from LES (Silvestrini *et al.*[1]). Since by definition a coherent vortex is a region of concentrated enstrophy, one way of analyzing these problems consists of using as a starting point the equation for the evolution of the resolved enstrophy. This was done recently in turbulent plane jets by da Silva and Pereira.[2] Compared to the enstrophy equation the resolved enstrophy equation has an additional new term, $D^{\mathrm{SGS}}=-\epsilon_{ijk}\overline{\Omega}_i\partial\tau_{kp}/\partial x_j\partial x_p$, the *SGS enstrophy dissipation*, which involves both the resolved vorticity $\overline{\Omega}_i$, and the subgrid-scale stresses τ_{ij}. Thus the effect of the subgrid-scale models on the evolution of the resolved enstrophy is described by this term.

In analogy with the SGS energy dissipation, the local SGS enstrophy dissipation can provide both a forward ($D^{\mathrm{SGS}}<0$) and a backward ($D^{\mathrm{SGS}}>0$) enstrophy transfer. In turbulent plane jets it is the forward enstrophy cascade that prevails,[2] i.e., $\langle D^{\mathrm{SGS}}(y)\rangle<0$ for all y, where y is the plane jet normal direction. Therefore the main effect of the SGS models on the evolution of the resolved enstrophy is to provide an additional mechanism of enstrophy dissipation. Several SGS models were tested by da Silva and Pereira[2] using both *a priori* and *a posteriori* tests in their ability to dissipate the correct amount of enstrophy. All tests showed that of all the models considered the dynamic Smagorinsky and filtered structure function models are the ones that lead to the best results in the prediction of the resolved vorticity field.

The purpose of this Letter is to extend this analysis into the more important and demanding context of wall flows. For this purpose classical *a priori* tests were conducted using DNS of a channel flow, and focusing on the dynamics of the resolved enstrophy as in Ref. 2. Whereas in LES of jets, wakes, and mixing layers it is reasonably easy to get the most important flow structures; wall flows display a complex tangle of interconnecting coherent and vortical structures such as low/high speed streaks, quasistreamwise and hairpin vortices that are not always easy to capture (Robinson[3]). Furthermore, the correct prediction of these vortical structures, in particular the quasistreamwise vortices, is crucial for the success of any LES involving near wall turbulence (Templeton *et al.*[4]). An additional complexity comes from the existence of a large mean velocity gradient which makes the flow inhomogeneous in the wall normal direction.

The numerical code used in the present simulations is a classical staggered finite difference Navier-Stokes solver using a centered second order scheme for spatial discretization and a third order Runge-Kutta scheme for temporal advancement. The pressure-velocity coupling is achieved by a fractional step method, where a Poisson equation is solved using spectral schemes in the homogeneous directions and a tridiagonal matrix solver in the wall normal direction. Full details are given in Orlandi.[5]

A direct numerical simulation (DNS) was carried out in a channel flows configuration with Reynolds number equal to $\mathrm{Re}_\tau=u_\tau\delta/\nu=180$, where u_τ is the friction velocity and δ is the channel half-height. The computational domain extends to $4\pi\delta\times 2\delta\times 4\pi\delta/3$ along the streamwise (x), normal (y), and spanwise (z) directions, respectively, as in Kim *et al.*,[6] and the resolution is $192\times 151\times 128$ grid points along these directions which gives a mesh spacing equal to $\Delta_x^+\times\Delta_y^+|_{\mathrm{wall}}/\Delta_y^+|_{\mathrm{center}}\times\Delta_z^+=11.84\times 0.56/4.38\times 5.87$.

The analysis was made using 100 instantaneous fields separated by $\Delta t^+\simeq 43$, taken after the flow has reached a statistically stationary state, which occurs after about $T^+=4300$. Figure 1 shows mean profiles of Reynolds stresses and root-mean-square vorticity fluctuations (in wall units) from the present simulation and the DNS from Kim *et al.*[6] The mean velocity (not shown), Reynolds stresses and root-mean-square vorticity fluctuations agree very well with the data from Kim *et al.*[6] Comparison of unidimensional kinetic energy spectra from the present DNS with similar spectra from Refs. 6–8 showed excellent agreement (not shown). Unidimensional enstrophy spectra at $y^+\approx 6$ from the present simulations are shown in Fig. 2(c), where one can see that

[a]Electronic mail: hauet@ist.utl.pt

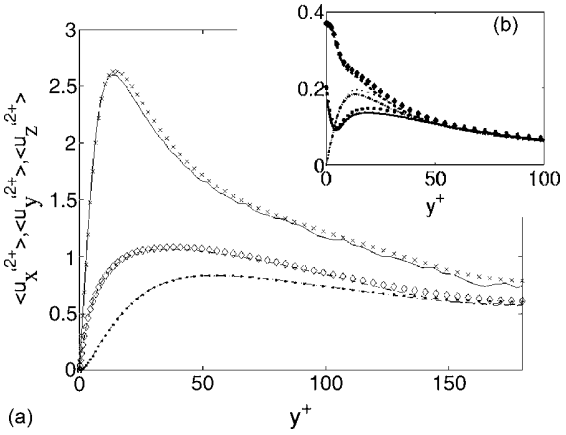

FIG. 1. Mean profiles of the Reynolds stresses (a) and root-mean-square vorticity fluctuations (b) for the present simulation (lines) compared to the DNS of Kim *et al.* (Ref. 6) (symbols).

the enstrophy decays smoothly at high wave numbers, a sign of a well resolved enstrophy field.

The separation between grid and subgrid-scales was made preferentially with 3D box filters, although 2D box filters and (2D) cutoff filters were also used. For the 2D box and cutoff filters the filter widths tested are equal to $\overline{\Delta}_x/\Delta_x = \overline{\Delta}_z/\Delta_z = 2,4,6$, while for the 3D box filter the filter widths along x and z are the same as in the 2D box filter and a further filtering is applied along the wall normal direction $\overline{\Delta}_y(y^+)/\Delta_y(y^+) = 2,4,6$. Notice that the 3D box filter is inhomogeneous along the wall normal direction. Mean profiles of the amount of kinetic energy contained at the subgrid-scales were computed (not shown). The profiles are very similar to the ones of Piomelli *et al.*[9] for similar filter widths and are representative of actual LES calculations. The amount of enstrophy in the SGS motions was also computed. At $y^+=25$ it amounts to 12%, 26%, 58% and 15%, 29%, 63%, for $\Delta/\Delta x = 2,4,6$ using a 2D and a 3D box filter, respectively.

Before detailing the dynamics of the resolved enstrophy transport equation it is important to outline the main features of the total (i.e., resolved+subgrid) enstrophy equation. The mean profiles of each one of its terms are shown in Fig. 2(a). As with the kinetic energy equation, there is a rough balance between production and dissipation, i.e., the advection and diffusion terms are in general less important and can be neglected for $y^+ > 20$. The maximum production and minimum dissipation are obtained at about $y^+ \approx 4$ and $y^+ \approx 7$, respectively, while the maximum kinetic energy production (not shown)[6] is obtained at $y^+ \approx 12$. Notice also that the enstrophy viscous dissipation tends to ≈ -0.006 when approaching the wall unlike the kinetic energy viscous dissipation (not shown), which has its minimum precisely at the wall.[6] Both the advection and viscous diffusion of enstrophy attain their minima at about $y^+ \approx 3$, and the former seems to be slightly more important for the enstrophy budget than is the viscous diffusion in the energy budget.

Budgets for the resolved or filtered enstrophy equation were computed using several filter types and sizes. Figure 2(b) shows the budget for the 3D box filter with $\Delta/\Delta x = 6$. Due to the filtering boundary conditions at $y^+=0$ using the 3D box filter the computation of the second derivative cannot be done accurately in the first four grid points, corresponding to $y^+ < 2.5$. For this reason the resolved enstrophy equation terms are not shown for these points. Compared to the enstrophy equation a new term arises, which represents the dissipation of resolved enstrophy caused by the subgrid-scale stresses, the *enstrophy SGS dissipation* (D^{SGS}). In the center of the channel ($y^+ \approx 180$, not shown), as in Ref. 2, the advection and viscous diffusion terms are negligible and the enstrophy production is balanced by the sum of the enstrophy viscous dissipation and the SGS enstrophy dissipation, i.e., there is a mean forward enstrophy cascade $\langle D^{\mathrm{SGS}}(y)\rangle < 0$.

The most important differences are to be found to be close to the wall for $y^+ < 30$, i.e., in the buffer and viscous layers. Indeed, for $y^+ < 30$ the magnitude of all the terms increases significantly and almost all the terms attain their minima/maxima at the buffer layer, the sole exception being the enstrophy viscous diffusion. In particular we see that the SGS enstrophy dissipation displays a minimum $\langle D^{\mathrm{SGS}}(y)\rangle$

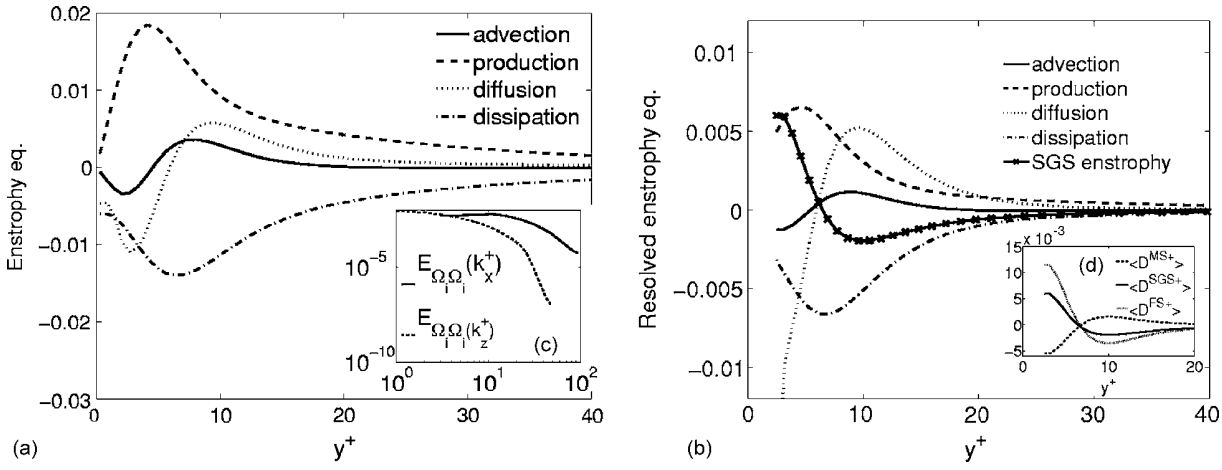

FIG. 2. Budgets for total (a) and resolved (b) enstrophy equation (in wall units). (b) was obtained with a 3D box filter with $\Delta/\Delta x = 6$, (c) displays the (streamwise and spanwise) unidimensional enstrophy spectra at $y^+ \approx 6$, and (d) shows the total ($D^{\mathrm{SGS+}}$), mean ($D^{\mathrm{MS+}}$) and fluctuating ($D^{\mathrm{FS+}}$) contributions of the SGS enstrophy dissipation.

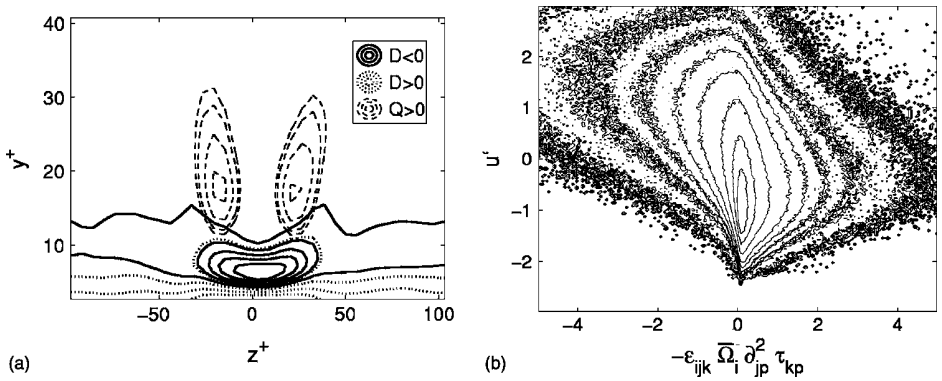

FIG. 3. (a) Contours of conditionally averaged fields showing regions of intense SGS enstrophy transfer and $Q>0$, where Q is a vortex-identification criterion (Dubief and Delcayre, Ref. 16); (b) joint probability density function between the SGS enstrophy dissipation and the filtered fluctuating streamwise velocity component at $y^+\simeq 8$ for the 3D box filter with $\Delta/\Delta x=6$.

<0 (enstrophy forward scatter) at about $y^+\approx 8$. For $y^+<7$ however, the SGS enstrophy dissipation exhibits a mean backward transfer $\langle D^{\mathrm{SGS}}(y)\rangle>0$. Qualitatively the same results were observed for the other filters (2D box and cutoff), in particular the 2D and 3D box filters give almost exactly the same results. The cutoff filter despite giving qualitatively similar results displays a smaller amount of mean forward and mean backscatter. Moreover, as expected and in agreement with Ref. 2, the total amount of SGS enstrophy dissipation increases with the filter size, for all filter types considered.

Härtel and Kleiser[10] decomposed the SGS (energy) dissipation into mean and fluctuating parts. They observed that near the wall the mean part of the SGS dissipation is one order of magnitude larger than the fluctuating part. Moreover, the fluctuating part exhibits a mean backscatter region near the wall. This fluctuating backscatter region was also observed in a pipe flow by Brun *et al.*[11] A similar decomposition was made here but applied to the SGS enstrophy dissipation. The total $\langle D^{\mathrm{SGS}}(y)\rangle$, mean $\langle D^{\mathrm{MS}}(y)\rangle = -\epsilon_{ijk}\langle\overline{\Omega}_i\rangle\partial\langle\tau_{kp}\rangle/\partial x_j\partial x_p$, and fluctuating $\langle D^{\mathrm{FS}}(y)\rangle = -\epsilon_{ijk}\langle\overline{\Omega}_i'\partial\tau_{kp}'/\partial x_j\partial x_p\rangle$ contributions of the SGS enstrophy dissipation were analyzed with $\langle D^{\mathrm{SGS}}(y)\rangle=\langle D^{\mathrm{MS}}(y)\rangle+\langle D^{\mathrm{FS}}(y)\rangle$, where the prime represents the fluctuating component of a given variable, e.g., $\overline{\Omega}_i=\langle\overline{\Omega}_i\rangle+\overline{\Omega}_i'$. Figure 2(d) shows results obtained with the 3D box filter with $\Delta/\Delta x=6$ using this decomposition. Unlike Härtel and Kleiser[10] the fluctuating contribution $\langle D^{\mathrm{FS}}(y)\rangle$ is more important than the mean part $\langle D^{\mathrm{MS}}(y)\rangle$ throughout the flow, even very close to the wall. It is surprising to see that the mean contribution to the SGS enstrophy dissipation has the opposite trend of the fluctuating contribution in terms of the resulting forward/backward enstrophy cascade. Whereas for $y^+>7$ the fluctuating contribution results in enstrophy forward scatter $\langle D^{\mathrm{FS}}(y)\rangle<0$, the mean contribution causes enstrophy backscatter $\langle D^{\mathrm{MS}}(y)\rangle>0$. Closer to the wall ($y^+<7$) this situation reverses, i.e., we have $\langle D^{\mathrm{FS}}(y)\rangle>0$ and $\langle D^{\mathrm{MS}}(y)\rangle<0$. It is not easy to explain the predominance of the fluctuating over the mean contribution for the total SGS enstrophy dissipation, however, a simple explanation can be given to the signal of $\langle D^{\mathrm{MS}}(y)\rangle$.

To explain this an analysis was made of the most important elements contributing to $\langle D^{\mathrm{MS}}(y)\rangle$. From all its 18 terms the computations showed that by far the most important term close to the wall is $\langle D^{\mathrm{MS}}(y)\rangle\approx\langle\overline{\Omega}_z\rangle\langle\partial_{yy}^2\tau_{xy}\rangle$, involving the second derivative of the SGS stress τ_{xy} in the wall normal direction and the spanwise vorticity Ω_z. This is not surprising recalling that in this flow $\langle\tau_{xy}\rangle$ and $\langle\Omega_z\rangle$ are the most important elements of the vorticity vector and subgrid-stresses tensor, respectively. Since the mean spanwise vorticity near the wall is $\langle\Omega_z\rangle\sim-\partial\langle u_x\rangle/\partial y<0$, the shape of $\langle\tau_{xy}(y)\rangle$ dictates the sign of $\langle D^{\mathrm{MS}}(y)\rangle$ near the wall. It was verified that as the distance from the wall increases, at about $y^+\approx 7$ the shape of $\langle\tau_{xy}(y)\rangle$ changes from $\langle\partial_{yy}^2\tau_{xy}\rangle>0$, into $\langle\partial_{yy}^2\tau_{xy}\rangle<0$, thus explaining the presence of a dominating enstrophy forward and backward scatter for $\langle D^{\mathrm{MS}}(y)\rangle$ in the regions $y^+<7$ and $y^+>7$, respectively.

Since the enstrophy SGS dissipation exhibits a particular behavior in the buffer layer it is interesting to see whether there is any link to the coherent structures present in this flow region. For this purpose conditional averages, similar to the ones of Piomelli *et al.*[9] were made in the channel flow, but focusing on the SGS enstrophy instead of the SGS energy transfer. One conditionally averaged field is shown in Fig. 3(a). This field was obtained using all the 100 instantaneous fields from the present data bank where about 1200 energy backscatter events were detected at $y^+=14$. The most intense regions of both kinetic energy (not shown) and enstrophy cascades occur close together, between two "legs" of quasistreamwise vortices. This result was confirmed also by the analysis of the correlations and joint probability density functions (JPDFs), where it could be observed that intense enstrophy and energy forward cascades take place in the same locations, in agreement with Ref. 2.

Another result confirms the existence of a link between regions of strong SGS enstrophy dissipation (enstrophy direct cascade) and the high-speed streaks (HSS). Visualizations of the three-dimensional fields showed that the most intense negative values of SGS enstrophy dissipation (forward enstrophy transfer) and positive streamwise velocity fluctuations (HSS) take place at the same locations. Indeed, an anticorrelation is found for $D^{\mathrm{SGS}}<0$ and $\bar{u}'>0$, reaching about 50%, in the region $4<y^+<17$, whereas outside this region the correlation is always positive and displays a constant and negligible value, of about 20%. The joint PDF between D^{SGS} and $\bar{u}'$ is shown in Fig. 3(b) at $y^+=8$. The plot shows that strong and negative values of SGS enstrophy dissipation (enstrophy forward scatter) are associated with re-

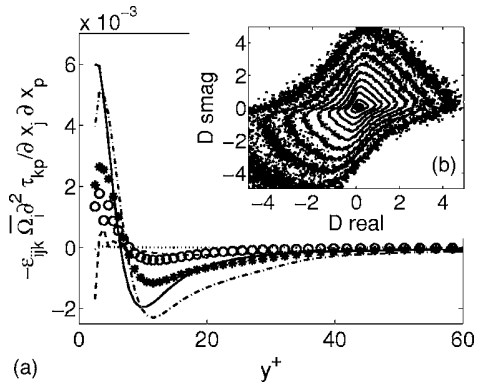

FIG. 4. (a) Mean profiles of the "real" (filtered DNS, solid line) and modelled SGS enstrophy dissipation using several models for the 3D box filter with $\Delta/\Delta x=6$. The models are the Smagorinsky (-.-), dynamic Smagorinsky (---), filtered structure function (…), scale-similarity (ooo), and mixed (***). (b) Joint probability density function between the "real" (filtered DNS) and the Smagorinsky modelled SGS enstrophy dissipation.

gions of intense positive streamwise velocity fluctuations (HSS), whereas strong SGS enstrophy backscatter is associated, although less strongly, with regions of negative streamwise velocity fluctuations [low speed streaks (LSS)]. Notice that the location $y^+=8$ defines the region where both the HSS and LSS, and the quasistreamwise vortices can usually be found (Robinson[3]). Thus, the dissipation of the quasistreamwise vortices caused by the SGS stresses takes place right at these high speed streak regions. Notice that a spatial correspondence between low-speed streaks (LSS) and regions of strong energy backscatter at $y^+\approx 2.8$ was previously observed by Schlatter *et al.*[8]

Finally, the filtered DNS and the modelled SGS enstrophy dissipation were compared using five classical SGS models: Smagorinsky (SMAG) with $C_s=0.1$, filtered structure function (FSF) (Ducros *et al.*[12]), dynamic Smagorinsky (DSMAG) (Lilly[13]), with clipping $C_s(y,t)\geqslant 0$, scale-similarity (SS) (Bardina *et al.*[14]), and mixed (MIX) (Meneveau and Katz[15]). For all but the DSMAG and SS models a Van Driest wall-damping function was used with $A^+=25$ (see Härtel and Kleiser[10] for details).

Figure 4(a) shows mean profiles of SGS enstrophy dissipations obtained with these models. Notice that from $y^+>7$ and throughout the centre of the channel the mean enstrophy SGS dissipation is negative for all models and filtered DNS, as in Ref. 2, but cannot be seen in the figure since the values are small compared to the values at $y^+\approx 8$. In this region in terms of enstrophy SGS dissipation the ranking of SGS models is the following, from least dissipative to most dissipative model: FSF, SS, DSMAG, MIX, (filtered DNS), and SMAG. In the majority of the buffer layer $(8<y^+<20)$ the ranking is almost the same: FSF, DSMAG, SS, MIX, (filtered DNS), and SMAG. Notice that this ranking is exactly the same found both in the *a priori* and *a posteriori* (LES) tests of Ref. 2. Finally, for $y^+<7$ all the models provide a mean enstrophy backscatter in the same proportion of their forward cascade in the previous region. In terms of enstrophy dissipation the most important flow region in wall bounded flows is the buffer layer, where the quasistreamwise vortices exist.[3] It follows that if this ranking of SGS models is confirmed by *a posteriori* tests, then the present results would indicate that in the buffer layer, from all SGS models considered, the FSF, SS and DSMAG will be the ones causing the smallest dissipation of resolved enstrophy, whereas the SMAG and MIX are likely be the most dissipative. It must be stressed however that these results need to be confirmed by LES, and moreover the influence of the Reynolds number in these results should be investigated in a future work.

Finally, the correlation between the filtered DNS and modelled SGS enstrophy dissipation was analyzed. Correlation coefficients were computed for all the models and the values obtained are very close to the values found in Ref. 2 for turbulent plane jets, e.g., about 55% for the SMAG, FSF, and DSMAG models. Similarly, at the center of the channel and in the buffer layer the JPDFs show the existence of a very high correlation for the exact and modelled forward SGS enstrophy transfer for the SMAG and FSF models (slightly less for the backward transfer) [see Fig. 4(b)] and an equally good correlation for both the forward and backward SGS enstrophy transfers in the DSMAG model (not shown).

This work was supported by the Ministério da Ciência e Tecnologia under Contracts No. SFRH/BPD/24464/2005 and No. SFRH/BPD/26576/2006.

[1] J. Silvestrini, P. Comte, and M. Lesieur, "DNS and LES of incompressible mixing layers developing spatially," in 10th Symposium on Turbulent Shear Flows, 1995.
[2] C. B. da Silva and J. C. F. Pereira, "The effect of subgrid-scale models on the vortices computed from large-eddy simulations," Phys. Fluids **16**, 4506 (2004).
[3] S. K. Robinson, "Coherent motions in the turbulent boundary layers," Annu. Rev. Fluid Mech. **23**, 601 (1991).
[4] J. A. Templeton, M. Wang, and P. Moin, "An efficient wall model for large-eddy simulation based on optimal control theory," Phys. Fluids **18**, 025101 (2006).
[5] P. Orlandi, *Fluid Flow Phenomena: A Numerical Toolkit* (Kluwer Academic, Dordrecht, 2000).
[6] J. Kim, P. Moin, and R. Moser, "Turbulent statistics in fully developed channel flow at low Reynolds number," J. Fluid Mech. **177**, 133 (1987).
[7] S. Stolz, N. A. Adams, and L. Kleiser, "An approximate deconvolution model for large-eddy simulation with application to incompressible wall-bounded flows," Phys. Fluids **13**, 2985 (2001).
[8] P. Schlatter, S. Stolz, and L. Kleiser, "Evaluation of high-pass filtered eddy-viscosity models for large-eddy simulation of turbulent flows," J. Turbul. **6**, 5 (2005).
[9] U. Piomelli, Y. Yu, and R. Adrian, "Subgrid-scale energy transfer and near-wall turbulence structure," Phys. Fluids **8**, 215 (1996).
[10] C. Härtel and L. Kleiser, "Analysis and modelling of subgrid-scale motions in near-wall turbulence," J. Fluid Mech. **356**, 327 (1998).
[11] C. Brun, R. Friedrich, and C. B. da Silva, "A nonlinear SGS model based on the spatial velocity increment: Application to LES of fully developed pipe flow and round turbulent jet," Theor. Comput. Fluid Dyn. **20**, 1 (2005).
[12] F. Ducros, P. Comte, and M. Lesieur, "Large-eddy simulation of transition to turbulence in a boundary layer developing spatially over a flat plate," J. Fluid Mech. **326**, 1 (1996).
[13] D. K. Lilly, "A proposed modification of the Germano subgrid-scale closure method," Phys. Fluids A **4**, 633 (1992).
[14] J. Bardina, J. H. Ferziger, and W. C. Reynolds, "Improved subgrid model for large-eddy simulation," AIAA Pap. No. 80-1357 (1980).
[15] S. Liu, C. Meneveau, and J. Katz, "On the properties of similarity subgrid-scale models as deduced from measurements in a turbulent jet," J. Fluid Mech. **275**, 83 (1994).
[16] Y. Dubief and F. Delcayre, "On coherent-vortex identification in turbulence," J. Turbul. **1**, 011 (2000).